Polarizability of shelled particles of arbitrary shape in lossy media with an application to hematic cells

José Luis Sebastián, Sagrario Muñoz, and Miguel Sancho

Departamento de Física Aplicada III, Facultad de Ciencias Físicas, Universidad Complutense, 28040 Madrid, Spain

Gabriel Álvarez

Departamento de Física Teórica II, Facultad de Ciencias Físicas, Universidad Complutense, 28040 Madrid, Spain

We show that within the dipole approximation the complex polarizability of shelled particles of arbitrary shape can be written as the volume of the particle times a weighted average of the electric field in the particle, with weights determined by the differences in permittivities between the shells and the external, possibly lossy media. To calculate the electric field we use an adaptive-mesh finite-element method which is very effective in handling the irregular domains, material inhomogeneities, and complex boundary conditions usually found in biophysical applications. After extensive tests with exactly solvable models, we apply the method to four types of hematic cells: platelets, T-lymphocytes, erythrocytes, and stomatocytes. Realistic shapes of erythrocytes and stomatocytes are generated by a parametrization in terms of Jacobi elliptic functions. Our results show, for example, that if the average polarizability is the main concern, a confocal ellipsoid may be used as a model for a normal erythrocyte, but not for a stomatocyte. A comparison with experimental electrorotation data shows quantitatively the effect of an accurate geometry in the derivation of electrical cell parameters from fittings of theoretical models to the experimental data.

I. INTRODUCTION

The general goal of this paper is to give a method for the calculation of the polarizability tensor α of a shelled piecewise homogeneous particle of arbitrary shape in lossy media. In response to an external electric field $\mathbf{E}_0$ the charge distributions of the particle and of the surrounding medium rearrange, in turn modifying the local field and therefore the total (far) field. This problem can be solved analytically for a spherical particle in a uniform external field, with the result that outside the sphere the total field is the superposition of the applied field $\mathbf{E}_0$ and a dipolar field of dipole moment $\mathbf{p} = \alpha \mathbf{E}_0$, where the polarizability α has a simple closed form in terms of the permittivities of the particle and of the medium (we consider only linear media) [1,2]. For particles of a general shape or when the external field is not uniform the exact response field need not be purely dipolar, but for many purposes higher multipolar fields can be neglected and the reaction of the particle can be approximated by an induced, effective dipole proportional to the external field. We will review later some shapes for which closed-form expressions of the polarizability have been found, but a precise computation of the tensor α for particles of arbitrary shape remains a difficult problem [3,4], which may require explicit computation of the fields.

In biophysics, the polarizability is an excellent monitor of the synchronization of cell growth in culture [5], and knowledge of α as a function of the frequency of the external field gives quantitative information on cell morphology [6]. In fact, our specific goal is the accurate determination of the polarizability of realistic models of hematic cells.

There are two main approaches to determine the polarizability of biological cells: from experimental dielectrophoresis (DEP) and electrorotation (ER) data and from *ab initio* calculations. The DEP force on a homogeneous, isotropic, dielectric, spherical cell is proportional to the real part of its effective polarizability, while in the concomitant ER experiments the imaginary part of the polarizability is derived from the rotation velocity of the cell in a rotating external field [7].

Ab initio formulas in terms of only electric and geometric parameters are known for the polarizability of particles of simple geometries and simple structure. The homogeneous dielectric sphere is a textbook example [2], and closed-form expressions can be found in the bibliography for spheroids, confocal spheroids, ellipsoids and confocal ellipsoids (in terms of nonelementary integrals), ellipsoids with certain anisotropic coatings, and pairs of spheres [8–14]. Although there is a general formula for the polarizability of a homogeneous particle of arbitrary shape [4], a generalization to realistic models of particles with complex geometries and complex structures (e.g., several layers of different lossy dielectric media) seems rather difficult to implement.

Expressions for the polarizability that involve explicitly surface charge distributions have also been published [6,15]. However, except in simple cases, these expressions are difficult to handle analytically because each unknown surface charge distribution is determined by an unbounded nonsymmetric integral operator. Boundary conditions at the interfaces of multishelled particles lead to even more complex systems of coupled integral equations. The comprehensive approach to DEP and ER proposed by Gimsa [16] for single-shell spheroids uses a finite-element ansatz and leads to a simplification of the calculation of the Clausius-Mossotti factor, but cannot be applied to small particles with relatively thick or highly conductive shells. Among the techniques to obviate some of these restrictions we mention the path-integral approach of Mansfield, Douglas, and Garboczi [3], which in addition to the polarizability gives the capacity and

the charge density of the system. For simple particles this path integral method is fast and reliable, and has been widely used. Even more recently Green and Jones [17] have proposed a method to extract induced multipole moments in a polarized particle by means of an expansion of the potential in spherical harmonics. However, in their application the authors consider only real permittivities and axisymmetric homogeneous particles.

Our approach is, in fact, straightforward and is summarized in Eq. (11) below: in essence we calculate the effective dipole moment of the cell from the internal electric field distribution, which in turn is determined by an adaptive finite-element numerical method that is able to achieve a uniform precision over very different length scales (e.g., typical membrane thicknesses and typical cytoplasm lengths). The method does not have have any restriction on the geometry or on the structure of the cell, although the computational effort certainly depends on these characteristics, as well as on the desired precision. We derive and discuss the main equation in Sec. II. In Sec. III we review the simple exactly solvable and the realistic cell models for T-lymphocytes, platelets, erythrocytes, and stomatocytes that we have used in our calculations. In Sec. IV we present our results and compare them with exact and experimental determinations of the polarizability. We discuss our conclusions in Sec. V.

II. EFFECTIVE DIPOLE MOMENT AND POLARIZABILITY

The calculation of the polarizability of a dielectric particle, in particular if the particle and the surrounding medium have losses, involves several subtleties and has been a subject of controversy. In the presence of losses the dipole moment induced in a particle by an external field experiences a phase delay with respect to the field due to the finite time required to establish a surface density of true charge on the interfaces. We define a complex effective dipole as the point dipole which, when immersed in the same dielectric medium as the original particle, produces the same dipolar field in magnitude and phase [18]. In effect, the particle can be replaced by this dipole for the calculation of electromechanical interactions with an external field. It has been shown that to a first-moment approximation this method gives the same results as the cumbersome and not always applicable Maxwell stress tensor method [19]. Therefore we follow the former approach and consider first the case of a homogeneous particle, then the case of shelled particles, and finally we make some remarks on the physical interpretation and use of our equations. Hereafter complex magnitudes will be denoted by a tilde.

A. Homogeneous particles

Let us assume that a periodic electric field $\widetilde{\mathbf{E}}_0 = \mathbf{E}_0 e^{-i\omega t}$ has been established in a homogeneous, isotropic, linear dielectric medium of permittivity ϵ_1 and conductivity σ_1—i.e., of complex permittivity $\widetilde{\epsilon}_1 = \epsilon_1 - i\sigma_1/\omega$—and that a homogeneous particle of complex permittivity $\widetilde{\epsilon}_2$ is placed into the field region while the sources of $\widetilde{\mathbf{E}}_0$ are kept constant.

In the surface S between the two dielectrics there is a surface density of equivalent polarization charges given by

$$\widetilde{\tau}_p = (\epsilon_2 - \epsilon_0)\widetilde{\mathbf{E}}_2 \cdot \mathbf{n} - (\epsilon_1 - \epsilon_0)\widetilde{\mathbf{E}}_1 \cdot \mathbf{n}, \tag{1}$$

where $\mathbf{n}$ is the unit normal to the surface, and because of the different conductivities at each side, there is also a surface density of true charge given by

$$\widetilde{\tau}_t = -i\frac{\sigma_2}{\omega}\widetilde{\mathbf{E}}_2 \cdot \mathbf{n} + i\frac{\sigma_1}{\omega}\widetilde{\mathbf{E}}_1 \cdot \mathbf{n}. \tag{2}$$

We define a net complex charge density $\widetilde{\tau}$, which includes both the polarization and true charges due to the two surfaces in contact:

$$\widetilde{\tau} = (\widetilde{\epsilon}_2 - \epsilon_0)\widetilde{\mathbf{E}}_2 \cdot \mathbf{n} - (\widetilde{\epsilon}_1 - \epsilon_0)\widetilde{\mathbf{E}}_1 \cdot \mathbf{n}. \tag{3}$$

Note that the contributions to the complex surface charge density $\widetilde{\tau}_p$ from the fields $\widetilde{\mathbf{E}}_1$ and $\widetilde{\mathbf{E}}_2$ are in phase with the fields, whereas the contributions to $\widetilde{\tau}_t$ are in quadrature. Since the normal components of the electric displacement and of the current density across the interface must be continuous,

$$\widetilde{\epsilon}_2\widetilde{\mathbf{E}}_2 \cdot \mathbf{n} = \widetilde{\epsilon}_1\widetilde{\mathbf{E}}_1 \cdot \mathbf{n}, \tag{4}$$

the net complex charge density is given by

$$\widetilde{\tau} = \epsilon_0 \frac{\widetilde{\epsilon}_2 - \widetilde{\epsilon}_1}{\widetilde{\epsilon}_1}\widetilde{\mathbf{E}}_2 \cdot \mathbf{n}, \tag{5}$$

which is a generalization of the corresponding expression for the polarization charge density at the interface between two lossless media. Therefore, in terms of fields and forces, we can consider that the polarized dielectric particle is equivalent to this charge distribution placed in vacuum. Since we have assumed that the particle is homogeneous, the potential it creates is fully determined by the surface charge:

$$\begin{aligned}\widetilde{\Phi}(\mathbf{r}) &= \frac{1}{4\pi\epsilon_0}\int_S \frac{\widetilde{\tau}(\mathbf{r}')}{|\mathbf{r} - \mathbf{r}'|}dS' \\ &= \frac{1}{4\pi\widetilde{\epsilon}_1}\int_S (\widetilde{\epsilon}_2 - \widetilde{\epsilon}_1)\frac{\widetilde{\mathbf{E}}_2(\mathbf{r}') \cdot \mathbf{n}'}{|\mathbf{r} - \mathbf{r}'|}dS'.\end{aligned} \tag{6}$$

(The difference $\widetilde{\epsilon}_2 - \widetilde{\epsilon}_1$ can be taken out of the integral, but we keep it under the integral sign to maintain uniformity with the generalized result derived in the next subsection.) Next we apply the Gauss theorem and the absence of free-volume charges $\boldsymbol{\nabla}' \cdot \widetilde{\mathbf{E}}_2(\mathbf{r}') = 0$ to write the potential as an integral over the volume V of the particle:

$$\widetilde{\Phi}(\mathbf{r}) = \frac{1}{4\pi\widetilde{\epsilon}_1}\int_V (\widetilde{\epsilon}_2 - \widetilde{\epsilon}_1)\widetilde{\mathbf{E}}_2(\mathbf{r}') \cdot \boldsymbol{\nabla}'\frac{1}{|\mathbf{r} - \mathbf{r}'|}dV'. \tag{7}$$

Finally, with the standard procedure with source (primed) coordinates referred to a center $\mathbf{r}_0$ inside the particle, we find that the dipolar part $\widetilde{\Phi}_2(\mathbf{r})$ of this potential, which dominates for $|\mathbf{r}| \gg |\mathbf{r}'|$, is

$$\widetilde{\Phi}_2(\mathbf{r}) = -\left(\boldsymbol{\nabla}\frac{1}{|\mathbf{r}-\mathbf{r}_0|}\right)\cdot\frac{1}{4\pi\widetilde{\epsilon}_1}\int_V(\widetilde{\epsilon}_2-\widetilde{\epsilon}_1)\widetilde{\mathbf{E}}_2(\mathbf{r}')dV'. \quad (8)$$

Since the potential created by a dipole $\widetilde{\mathbf{p}}$ in a medium of permittivity $\widetilde{\epsilon}_1$ is given by

$$\widetilde{\Phi}_2(\mathbf{r}) = -\left(\boldsymbol{\nabla}\frac{1}{|\mathbf{r}-\mathbf{r}_0|}\right)\cdot\frac{\widetilde{\mathbf{p}}}{4\pi\,\mathrm{Re}(\widetilde{\epsilon}_1)}, \quad (9)$$

we find that, in our dipolar approximation, the response of the particle is equivalent to that of an effective dipole

$$\widetilde{\mathbf{p}}_{\mathrm{eff}} = \frac{\mathrm{Re}(\widetilde{\epsilon}_1)}{\widetilde{\epsilon}_1}\int_V(\widetilde{\epsilon}_2-\widetilde{\epsilon}_1)\widetilde{\mathbf{E}}_2(\mathbf{r}')dV' \quad (10)$$

and therefore to an effective polarizability tensor, which can be calculated from

$$\widetilde{\alpha}_{\mathrm{eff}}\widetilde{\mathbf{E}}_0 = \frac{\mathrm{Re}(\widetilde{\epsilon}_1)}{\widetilde{\epsilon}_1}\int_V(\widetilde{\epsilon}_2-\widetilde{\epsilon}_1)\widetilde{\mathbf{E}}_2(\mathbf{r}')dV'. \quad (11)$$

B. Shelled particles

We will show now that in the case of shelled particles Eq. (11) continues to be valid with the understanding that the permittivity ϵ_2 and conductivity σ_2 in $\widetilde{\epsilon}_2$ may have different constant values in the different homogeneous regions of the particle. For this purpose, consider a particle with an outer (*o*) shell bounded by the outer surface S_o and by the inner surface S_i, which in turn bounds the inner core (*i*). Applying twice the reasoning that led to Eq. (5) we find that there are the charge densities

$$\widetilde{\tau}_o = \epsilon_0\frac{\widetilde{\epsilon}_o-\widetilde{\epsilon}_1}{\widetilde{\epsilon}_1}\widetilde{\mathbf{E}}_o\cdot\mathbf{n}_o, \quad (12)$$

$$\widetilde{\tau}_i = \epsilon_0\frac{\widetilde{\epsilon}_i-\widetilde{\epsilon}_o}{\widetilde{\epsilon}_o}\widetilde{\mathbf{E}}_i\cdot\mathbf{n}_i, \quad (13)$$

at the outer and inner surfaces, respectively, and a total complex potential which is the sum of two terms of the type given by Eq. (6):

$$\widetilde{\Phi}(\mathbf{r}) = \frac{1}{4\pi\widetilde{\epsilon}_1}\int_{S_o}(\widetilde{\epsilon}_o-\widetilde{\epsilon}_1)\frac{\widetilde{\mathbf{E}}_o(\mathbf{r}')\cdot\mathbf{n}_o'}{|\mathbf{r}-\mathbf{r}'|}dS_o'$$

$$+ \frac{1}{4\pi\widetilde{\epsilon}_o}\int_{S_i}(\widetilde{\epsilon}_i-\widetilde{\epsilon}_o)\frac{\widetilde{\mathbf{E}}_i(\mathbf{r}')\cdot\mathbf{n}_i'}{|\mathbf{r}-\mathbf{r}'|}dS_i'. \quad (14)$$

Next we apply the Gauss theorem to the first surface integral, which yields a volume integral over V_o minus a surface term over S_i. Note, however, that the outward normal at S_i from V_o is minus the outward normal from V_i. Therefore we have

$$\widetilde{\Phi}(\mathbf{r}) = \frac{1}{4\pi\widetilde{\epsilon}_1}\int_{V_o}(\widetilde{\epsilon}_o-\widetilde{\epsilon}_1)\widetilde{\mathbf{E}}_o(\mathbf{r}')\cdot\boldsymbol{\nabla}'\frac{1}{|\mathbf{r}-\mathbf{r}'|}dV_o'$$

$$+ \frac{1}{4\pi\widetilde{\epsilon}_1}\int_{S_i}(\widetilde{\epsilon}_o-\widetilde{\epsilon}_1)\frac{\widetilde{\mathbf{E}}_o(\mathbf{r}')\cdot\mathbf{n}_i'}{|\mathbf{r}-\mathbf{r}'|}dS_i'$$

$$+ \frac{1}{4\pi\widetilde{\epsilon}_o}\int_{S_i}(\widetilde{\epsilon}_i-\widetilde{\epsilon}_o)\frac{\widetilde{\mathbf{E}}_i(\mathbf{r}')\cdot\mathbf{n}_i'}{|\mathbf{r}-\mathbf{r}'|}dS_i'. \quad (15)$$

The continuity of the normal components of the electric displacement and of the current density across the surface S_i,

$$\widetilde{\epsilon}_o\widetilde{\mathbf{E}}_o\cdot\mathbf{n}_i = \widetilde{\epsilon}_i\widetilde{\mathbf{E}}_i\cdot\mathbf{n}_i, \quad (16)$$

allows us to replace $\widetilde{\mathbf{E}}_o\cdot\mathbf{n}_i$ in the first surface integral by $(\widetilde{\epsilon}_i/\widetilde{\epsilon}_o)\widetilde{\mathbf{E}}_i\cdot\mathbf{n}_i$ and group both surface integrals:

$$\widetilde{\Phi}(\mathbf{r}) = \frac{1}{4\pi\widetilde{\epsilon}_1}\int_{V_o}(\widetilde{\epsilon}_o-\widetilde{\epsilon}_1)\widetilde{\mathbf{E}}_o(\mathbf{r}')\cdot\boldsymbol{\nabla}'\frac{1}{|\mathbf{r}-\mathbf{r}'|}dV_o'$$

$$+ \frac{1}{4\pi\widetilde{\epsilon}_1}\int_{S_i}(\widetilde{\epsilon}_i-\widetilde{\epsilon}_1)\frac{\widetilde{\mathbf{E}}_i(\mathbf{r}')\cdot\mathbf{n}_i'}{|\mathbf{r}-\mathbf{r}'|}dS_i'. \quad (17)$$

Finally, we apply the Gauss theorem to the last surface integral to arrive at

$$\widetilde{\Phi}(\mathbf{r}) = \frac{1}{4\pi\widetilde{\epsilon}_1}\int_{V_o}(\widetilde{\epsilon}_o-\widetilde{\epsilon}_1)\widetilde{\mathbf{E}}_o(\mathbf{r}')\cdot\boldsymbol{\nabla}'\frac{1}{|\mathbf{r}-\mathbf{r}'|}dV_o'$$

$$+ \frac{1}{4\pi\widetilde{\epsilon}_1}\int_{V_i}(\widetilde{\epsilon}_i-\widetilde{\epsilon}_1)\widetilde{\mathbf{E}}_i(\mathbf{r}')\cdot\boldsymbol{\nabla}'\frac{1}{|\mathbf{r}-\mathbf{r}'|}dV_i'. \quad (18)$$

Each of these two integrals has the same form as Eq. (7), and therefore the respective contributions to the polarizability can be calculated by the same method, which gives

$$\widetilde{\alpha}_{\mathrm{eff}}\widetilde{\mathbf{E}}_0 = \frac{\mathrm{Re}(\widetilde{\epsilon}_1)}{\widetilde{\epsilon}_1}\int_{V_o}(\widetilde{\epsilon}_o-\widetilde{\epsilon}_1)\widetilde{\mathbf{E}}_o(\mathbf{r}')dV_o'$$

$$+ \frac{\mathrm{Re}(\widetilde{\epsilon}_1)}{\widetilde{\epsilon}_1}\int_{V_i}(\widetilde{\epsilon}_i-\widetilde{\epsilon}_1)\widetilde{\mathbf{E}}_i(\mathbf{r}')dV_i'. \quad (19)$$

This equation, as we anticipated, can be rewritten as Eq. (11) with the understanding that in the outer region V_o the permittivity of the particle $\widetilde{\epsilon}_2=\widetilde{\epsilon}_o$ and the field $\widetilde{\mathbf{E}}_2(\mathbf{r}')=\widetilde{\mathbf{E}}_o(\mathbf{r}')$, while in the inner region V_i the permittivity of the particle $\widetilde{\epsilon}_2=\widetilde{\epsilon}_i$ and the field $\widetilde{\mathbf{E}}_2(\mathbf{r}')=\widetilde{\mathbf{E}}_i(\mathbf{r}')$. Hereafter we follow this convention and will refer always to Eq. (11). The generalization of this result to multiple shells is straightforward.

C. General remarks

We would like to stress a few points regarding the derivation and practical use of Eq. (11). For a homogeneous particle Eq. (11) can be written as

$$\widetilde{\alpha}_{\mathrm{eff}}\widetilde{\mathbf{E}}_0 = \frac{\mathrm{Re}(\widetilde{\epsilon}_1)}{\widetilde{\epsilon}_1}(\widetilde{\epsilon}_2-\widetilde{\epsilon}_1)V\langle\mathbf{E}_2\rangle, \quad (20)$$

where V is the volume of the particle and $\langle\mathbf{E}_2\rangle$ is the average field in the particle. First note that both factors

$\epsilon_0(\widetilde{\epsilon}_2 - \widetilde{\epsilon}_1)/\widetilde{\epsilon}_1$ and $\mathrm{Re}(\widetilde{\epsilon}_1)/\epsilon_0$ must be included in the definition of $\widetilde{\mathbf{p}}_{\mathrm{eff}}$. The first factor can be physically understood from the analogy of a body immersed in a fluid under a gravitational field: to calculate the net force we must subtract a buoyancy term which is equivalent to the negative term on the right-hand side of the expression for the surface charge, Eq. (5). The second factor is a consequence of the fact that the equivalent charges and dipole are considered to be in vacuum, and therefore the external field has to be multiplied by the relative inductive factor between vacuum and medium.

If both media are loss free, the effective dipole is real and given by

$$\mathbf{p}_{\mathrm{eff}} = \int_V (\epsilon_2 - \epsilon_1)\mathbf{E}_2(\mathbf{r}')dV', \tag{21}$$

and the force can be obtained as minus the gradient of the energy U of the particle in the field [2], where

$$U = -\frac{1}{2}\mathbf{p}_{\mathrm{eff}} \cdot \mathbf{E}_0 = -\frac{1}{2}\int_V (\epsilon_2 - \epsilon_1)\mathbf{E}_2(\mathbf{r}')dV' \cdot \mathbf{E}_0$$

$$= -\frac{1}{2}\alpha_{\mathrm{eff}}|\mathbf{E}_0|^2. \tag{22}$$

However, in lossy media $\widetilde{\mathbf{p}}_{\mathrm{eff}}$ is complex, Eq. (10) must be used, and the force produced by the field on the dielectric particle is

$$\mathbf{F} = \frac{1}{2}\,\mathrm{Re}[(\widetilde{\mathbf{p}}_{\mathrm{eff}} \cdot \boldsymbol{\nabla})\widetilde{\mathbf{E}}_0^*]. \tag{23}$$

As to the use of Eq. (11), the procedure is as follows: we apply the external field $\widetilde{\mathbf{E}}_0$, calculate numerically the field $\widetilde{\mathbf{E}}_2$ as described in Sec. IV, perform the integration in Eq. (11), and thus obtain three components of the effective polarizability tensor. With three orientations of the external field we can determine the full tensor.

The numerical calculations in Sec. IV will give the field both inside and in a certain region outside the particle. As we stated in the Introduction, in principle the polarizability could be extracted from a multipole expansion of the field (or of the potential) outside the particle. But for complex permittivities and realistic cell shapes other than spherical, this multipole expansion is not a straightforward process and requires both a careful determination of the radius of the spherical surface on which the field is to be integrated and an interpolation of the field at each point of the surface in terms of the fields at neighboring nodes. A convenient radius becomes especially difficult to determine when the particle is immersed in an external lossy medium and when the electric field is highly nonuniform [17]. Conversely, we remark that the integration in Eq. (11) is performed only over the volume V of the particle, where the field is very accurately determined by a finite-element method with a highly refined and adapted mesh. This accurate field in turn permits the calculation of several magnitudes of biophysical interest such as the induced transmembrane potential or the Maxwell stress tensor.

III. CELL MODELS

We will focus on the polarizability of four characteristic types of hematic cells: platelets, T-lymphocytes, erythrocytes, and type-II stomatocytes. The first three cells will be studied in their normal state, whereas the type-II stomatocyte is in fact a severely altered state of an erythrocyte whose complex geometry provides a good testing ground for our approach.

There is a specific feature pertaining to the polarizability of biological cells: the cell and surrounding medium electrical properties make the membrane a locus of high-field amplification, whereas typical membrane thicknesses are much smaller than typical cytoplasmic lengths. This scale problem poses a challenge to standard numerical methods. Therefore, before embarking in more realistic calculations, we have checked our method by comparing its results with simpler exactly solvable models. We discuss in separate subsections the exactly solvable and the more realistic models that we have used. With the exception of the experimental results quoted in Sec. IV C, we assume that the (solvable or realistic) cell models are immersed in an external continuous medium formed by an electrolyte with the dielectric properties of physiological saline; i.e., we take $\widetilde{\epsilon}_1 = \epsilon_r\epsilon_0 - i\sigma/\omega$ with a relative permittivity $\epsilon_r = 80$ and a conductivity $\sigma = 0.12$ S/m.

Note also that the derivation of Eq. (19) neglects any ion diffusion effects. This assumption will be justified if the thickness of the diffusion layer (the Debye screening length λ_D) is smaller than the smallest characteristic length in the structure (the thickness of the membrane δ). At the physiological conditions considered in this work and with a diffusion coefficient $D = 10^{-9}$ m^2 s^{-1} [20], the ratio is $\lambda_D/\delta = 0.48$. Due to this small value of the Debye length, the electric double layer is locally nearly planar and fits closely the erythrocyte shape. Although the potential is strongly screened, the internal field distribution should correspond essentially to the solution of the Laplace equation which we use in our calculations. The comparison with experimental results in Sec. IV C supports the validity of this assumption. Finally we also assume that the cell shape is not modified and does not suffer instabilities in the presence of the external field, and therefore we do not apply the Debye-Hückel theory, which may be needed in the presence of strong electrolytes where these effects are more prone to occur [21,22].

A. Exactly solvable models

We have considered three exactly solvable models: a homogeneous sphere, a homogeneous ellipsoid, and a shelled confocal ellipsoid [11], with the required modifications for lossy media explained in the previous section after the derivation of Eq. (11). Incidentally, the permittivity of the medium is factored out in the definition of polarizability used in Ref. [11]; our Eqs. (24), (25), and (28) below include both the correction for lossy media and this factor, so that these equations are consistent with the more standard convention that we use in this paper. The dimensions and electrical parameters of these models have been chosen to match to the extent possible regions of hematic cells.

The polarizability of a homogeneous sphere of radius a is

$$\widetilde{\alpha} = 3V \operatorname{Re}(\widetilde{\epsilon}_1) \frac{\widetilde{\epsilon}_2 - \widetilde{\epsilon}_1}{\widetilde{\epsilon}_2 + 2\widetilde{\epsilon}_1}, \qquad (24)$$

where $V = 4\pi a^3/3$ is the volume of the particle. In our calculations we have taken $a = 3$ μm and $\widetilde{\epsilon}_2 = \epsilon_r \epsilon_0 - i\sigma/\omega$, with $\epsilon_r = 50$ and $\sigma = 0.53$ S/m, which correspond to a typical sphere of cytoplasm.

The polarizability of a homogeneous ellipsoid of semiaxes a, b, and c in a field parallel to the c axis is

$$\widetilde{\alpha}_c = V \operatorname{Re}(\widetilde{\epsilon}_1) \frac{\widetilde{\epsilon}_2 - \widetilde{\epsilon}_1}{\widetilde{\epsilon}_1 + L_c(\widetilde{\epsilon}_2 - \widetilde{\epsilon}_1)}, \qquad (25)$$

where $V = 4\pi abc/3$ is the volume of the particle and

$$L_c = \frac{abc}{2} \int_0^\infty \frac{dq}{(c^2 + q)\sqrt{(a^2 + q)(b^2 + q)(c^2 + q)}}, \qquad (26)$$

with analogous expressions for the other two axes. (If $a = b = c$, then $L_a = L_b = L_c = 1/3$ and we recover the expression for the sphere.) In our calculations we have taken $a = b = 1.2$ μm, $c = 0.38$ μm, $\epsilon_r = 57$, and $\sigma = 0.5$ S/m, which are typical parameters of the cytoplasm of a platelet.

Inner (i) and outer (o) confocal ellipsoids can be described by

$$\frac{x^2}{a_k^2} + \frac{y^2}{b_k^2} + \frac{z^2}{c_k^2} = 1 \quad (k = i, o), \qquad (27)$$

where $a_o^2 - a_i^2 = b_o^2 - b_i^2 = c_o^2 - c_i^2 = \xi > 0$. The polarizability in a field parallel to the c_k axes is

$$\widetilde{\alpha}_c = V \operatorname{Re}(\widetilde{\epsilon}_1) \frac{(\widetilde{\epsilon}_o - \widetilde{\epsilon}_1)[\widetilde{\epsilon}_o + (\widetilde{\epsilon}_i - \widetilde{\epsilon}_o)(L_{c_i} - rL_{c_o})] + r\widetilde{\epsilon}_o(\widetilde{\epsilon}_i - \widetilde{\epsilon}_o)}{[\widetilde{\epsilon}_o + (\widetilde{\epsilon}_i - \widetilde{\epsilon}_o)(L_{c_i} - rL_{c_o})][\widetilde{\epsilon}_1 + (\widetilde{\epsilon}_o - \widetilde{\epsilon}_1)L_{c_o}] + rL_{c_o}\widetilde{\epsilon}_o(\widetilde{\epsilon}_i - \widetilde{\epsilon}_o)}, \qquad (28)$$

where $V = 4\pi a_o b_o c_o/3$ is the volume of the particle and $r = a_i b_i c_i/a_o b_o c_o$ is the fraction of this volume occupied by the inner ellipsoid. In our calculations we have taken as geometric parameters $a_i = b_i = 3.9$ μm, $c_i = 1.3344$ μm, and $\xi = 0.0343658$, which give the same volume of cytoplasm and the same volume of membrane as our realistic model of a normal erythrocyte. The electrical parameters in the complex permittivity of the cytoplasm, $\widetilde{\epsilon}_i$, are the same as in the homogeneous sphere example. The electrical parameters in the complex permittivity of the membrane $\widetilde{\epsilon}_o$ are $\epsilon_r = 5$ and $\sigma = 10^{-6}$ S/m.

B. Realistic models

T-lymphocytes have spherical shape, a thin membrane, and a spherical nucleus which fills about 60% of the total volume. Our model for this type of cell will be a spherical core of radius 3 μm and relatively high conductivity covered by a thin spherical shell of thickness 5 nm and five orders of magnitude less conductive than the inner region [23,24].

Platelets have a distinct inner structure with several vesicles [25] and therefore would be expected to have a more complex dispersion relation. Several geometries have been proposed to study the dielectric properties of the particle—e.g., a spherical single-shell model [26], a cubically structured model [27], and rectangular parallelepipeds [28]. We have chosen a model comprised by an inner homogeneous ellipsoid for the cytoplasm with semiaxes $a = b = 1.2$ μm, $c = 0.38$ μm, and a membrane with a constant thickness of 7 nm. (Confocal ellipsoids bound an unrealistic nonuniform membrane.)

A normal human erythrocyte under physiological conditions assumes a biconcave shape (discocyte) of approximately 7.8 μm in diameter, with a membrane whose thickness is of the order of 8 nm [29]. However, it has also been known for more than 50 years [30] that a variety of agents can modify this discoid shape systematically and reversibly. One set of agents, including cationic amphipaths, low salt, low pH, and cholesterol depletion, induces altered shapes called stomatocytes [31,32]. Instead of having the rounded central pallor of a normal red cell, a stomatocyte has a centrally located linear slit or stoma ("fish mouth"). The cell maintains the same volume of the original erythrocyte, and the shape alteration has been described by the fluctuations of a single, polymerized membrane [33]. This cell attracts great interest as it is part of the stomatocyte-discocyte-echinocyte sequence of the human red blood cell [34,35]. In previous works [36,37] we have analyzed the role played by the geometry of erythrocytes in their response to electromagnetic fields, and in Ref. [38] we have proposed a slight generalization of the parametrization that Kuchel and Fackerell [39] gave for normal erythrocytes. Our generalization, which can describe continuous deformations from the normal shape to altered shapes like stomatocytes, can be written as

$$\mathbf{r}(u, \phi) = \left(\frac{\ell}{2} \operatorname{cn}(u|m) \cos \phi, \frac{\ell}{2} \operatorname{cn}(u|m) \sin \phi, \right.$$
$$\left. \pm h \operatorname{sn}(u|m) \left(\frac{\operatorname{dn}(u|m)}{\operatorname{dn}(U|m)} \right)^p \right), \qquad (29)$$

where $\operatorname{sn}(u|m)$, $\operatorname{cn}(u|m)$, and $\operatorname{dn}(u|m)$ are Jacobi elliptic functions [40], $U = K(m)$ is the corresponding elliptic integral, $u \in [0, U]$, $\phi \in [0, 2\pi]$, ℓ is the diameter of the cell, h is the semiheight at the center, and m and p can be used to control the gross features of the shape. Using different values of h, m, and p for the upper ($+h$) and lower ($-h$) parts of the
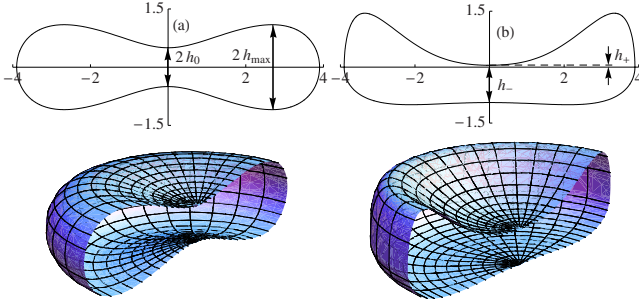
FIG. 1. (Color online) (a) Normal biconcave erythrocyte of diameter $\ell = 7.8$ μm, maximum height $2h_{max} = 2.18$ μm, height at the center $2h_0 = 1$ μm, and volume $V_{cyt} = 85$ $(\mu m)^3$, which corresponds to a value of $p = 1$ and $m = 0.9447$ for both the upper and lower half of the cell in Eq. (29). (b) Stomatocyte of the same volume, height at the center, and diameter modeled with $p = 3$, $h_+ = 0.05$ μm, and $m = 0.949$ for the upper part and $p = 2$, $h_- = 0.95$ μm, and $m = 0.472$ for the lower part of the cell in Eq. (29). The membranes of thickness 8 nm are not shown.

cell we can generate asymmetric cells like the stomatocyte. With this explicit parametrization we calculate the outer surface $\mathbf{r}_\delta(u, \phi)$ of the uniform membrane by shifting the surface $\mathbf{r}(u, \phi)$ a constant distance δ along the outer normal at each point—that is,

$$\mathbf{r}_\delta(u, \phi) = \mathbf{r}(u, \phi) + \delta \frac{(\partial \mathbf{r}/\partial \phi) \times (\partial \mathbf{r}/\partial u)}{\|(\partial \mathbf{r}/\partial \phi) \times (\partial \mathbf{r}/\partial u)\|}. \quad (30)$$

We refer to Fig. 1 and Table I for the numerical values that we have used and to Ref. [38] for further details.

IV. RESULTS

The field $\tilde{\mathbf{E}}_2$ within a realistic cell can only be obtained with the help of numerical methods. In this work we have used the adaptive-mesh finite-element software ANSOFT [41], which is very effective in handling the irregular domains, material inhomogeneities, and complex boundary conditions usually found in electromagnetism [42,43] and in biomedical problems [44–46], as well as the nonuniform meshing required by the cytoplasm and the membrane [47]. Although this last difficulty can be overcome with hybrid numerical techniques that couple the finite-element method with the boundary element method [48,49], the adaptive approach can be readily applied also to any number of neighboring particles within an arbitrarily shaped radiation region.

In our calculations the cell is centered in a cube (the radiation region) large enough to ensure the homogeneity of the external field and to achieve a good compromise between accuracy and computing resources. This region is filled with the external medium described in Sec. III. We implement perfectly matched layers as "absorbing boundary conditions" that mimic continued radiation in free space, so that any incident energy not absorbed by the cell is not reflected back into the model. As a technical improvement, we insert additional vertices by means of two virtual regions (objects within the radiation region with the same material assignment as the external medium) that surround the cell and contribute to the generation of a clean mesh. An impinging external field of magnitude $E_0 = 1$ V/m is generated by applying a drop voltage of variable frequency and constant magnitude over two opposite faces of the cube that limits the radiation region.

We have found that to reach a uniformly accurate result for the electric field, the final mesh required around 50 000 and 7500 tetrahedra per cubic micron of membrane and cytoplasm, respectively. A typical computing time for the most complex model—a stomatocyte—in a 3.4-GHz microprocessor is of the order of 800 min.

A. Exactly solvable models

Two factors determine the precision that can be achieved with this method for a particle of generic shape: the dipole approximation, which is intrinsic to the method, and the accuracy in the numerical calculation of the field. To be precise, the calculation of the field is an iterative process which stops when the difference between the integral of the modulus squared of the field in two consecutive iterations is less than a convergence criterion $\Delta \varepsilon$ [41]. Figure 2(a) shows the exact and numerical values of the real and imaginary parts of the (scalar) polarizability of the homogeneous sphere described in Sec. III A as a function of the frequency in the range from 10 kHz to 3 GHz. Figure 2(b) shows the same magnitudes for the homogeneous revolution ellipsoid along the two principal axes y and z. Finally, Fig. 3 shows the complex polarizability of the confocal ellipsoid test cell again along the two different principal axes. In these calculations we have set typically $\Delta \varepsilon = 10^{-9}$ and we have obtained errors in the real and imaginary parts of the polarizability less than 1.5%. A smaller value of $\Delta \varepsilon$ increases the precision of the polarizability at the cost of an increased computing

TABLE I. Electrical and geometrical parameters of human T-lymphocytes, platelets, normal erythrocytes, and type-II stomatocytes.

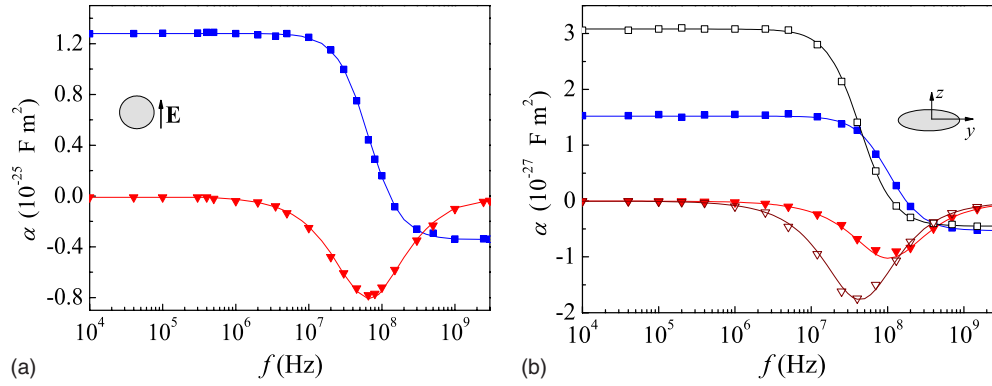| Cell	Membrane				Cytoplasm		
	ϵ_r	σ (10^{-6} S/m)	δ (nm)	Vol. (μm^3)	ϵ_r	σ (S/m)	Vol. (μm^3)
T-lymphocyte	7.63	10	5	0.57	50	1	113.10
Platelet	9	2	7	0.07	57	0.5	2.29
Erythrocyte	5	1	8	1.01	50	0.53	85.02
Stomatocyte	5	1	8	1.12	50	0.53	85.09

FIG. 2. (Color online) Comparison between the exact (solid lines) and our numerical results for the complex polarizability of (a) a lossy homogeneous sphere and (b) a lossy homogeneous ellipsoid, as a function of the frequency f of the applied external field. The exact results are given by Eqs. (24) and (25), respectively. The squares mark the real parts of the polarizability, while the triangles mark the imaginary parts. Open markers in (b) correspond to α_y and closed markers to α_z.

time which depends on the necessary refinements of the mesh.

B. Realistic models

The simple spherical geometry of the T-lymphocyte, a coated sphere, is the particular case $a=b=c$ of a coated confocal ellipsoid, and therefore we can also find the exact values of the polarizability with Eq. (28). Figure 4 shows a comparison of this analytical solution with our numerical values.

As the membrane of the platelet has a uniform thickness, there is no analytical solution for the polarizability that could be used for comparison. However, we have taken advantage of the revolution symmetry of the platelet around the z axis and implemented the boundary-element method [19] to obtain the polarizability along this axis. Figure 5(a) shows a comparison of the boundary-element polarizability with the method proposed in this work. Figure 5(b) shows the results for the polarizability along the long axis of the platelet. The very small values are due to the reduced volume of the platelet compared with the other cells of this study.

In theoretical studies of erythrocytes it is a common practice [50–52] to use confocal ellipsoids as a substitute for a realistic erythrocyte shape, thus avoiding the geometrical complexity of the real cell. We have calculated the polarizability of an erythrocyte using the realistic cell shape generated by Eq. (29) and compared the values with exact results for a confocal ellipsoid when the external field is applied along the principal axes. Since the confocal structure does not enclose a membrane of constant thickness, we have taken as a criterion for comparison that both cells have the same membrane volume. Figure 6(a) shows that both models give not too different polarizabilities along the z axis. Note that in this configuration the internal field distribution is very similar in both cells due to the continuity of the normal component of the displacement field through the membrane interface, where the field is amplified and therefore higher. More noticeable differences are observed in Fig. 6(b) corresponding to a polarization along the y axis. In this case the requirement of continuity of the tangential component of the field through the membrane surface of the biconcave shape leads to very different field distributions.
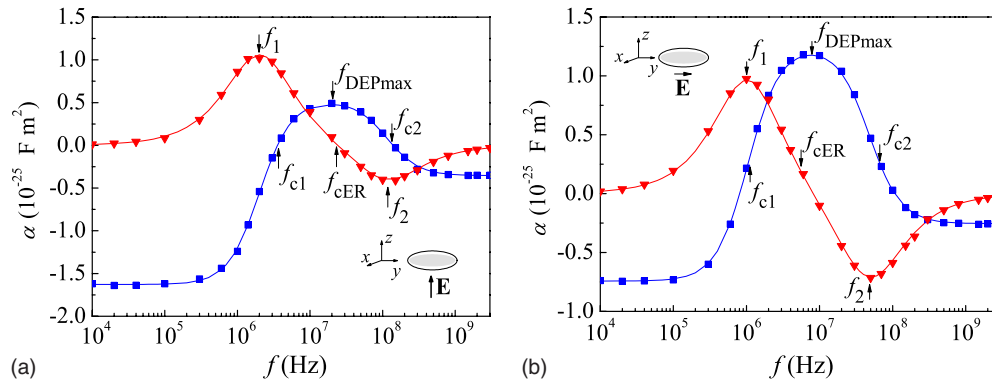

FIG. 3. (Color online) Comparison between the exact (solid lines) and our numerical results for the complex polarizability of a lossy confocal ellipsoid along (a) the minor z axis and (b) the major y axis, as a function of the frequency f of the applied external field. The exact results are given by Eq. (28). The squares mark the real parts of the polarizability, while the triangles mark the imaginary parts. The frequencies f_1 and f_2 correspond to the positive maximum and negative minimum of $\text{Im}(\widetilde{\alpha})$, respectively, whereas f_{c1} and f_{c2} are the crossover frequencies of $\text{Re}(\widetilde{\alpha})$. It is a well-known fact in dielectrophoresis that the crossover frequency f_{cER} of the ER spectrum is equal to the frequency f_{DEPmax} of maximum DEP force.
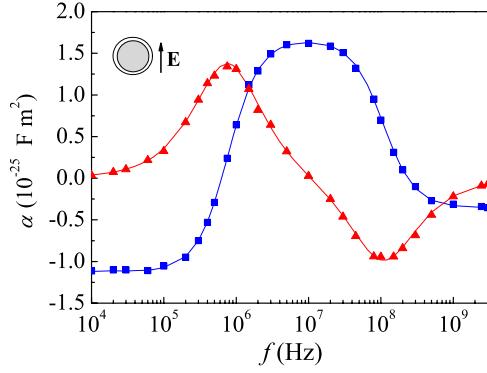
FIG. 4. (Color online) Comparison between the exact (solid lines) and our numerical results for the complex polarizability of a T-lymphocyte as a function of the frequency f of the applied external field. The exact results are given by Eq. (28) with $a=b=c$. The squares mark the real part of the polarizability, while the triangles mark the imaginary part.

As our last example, we have calculated the polarizability of the type-II stomatocyte described in Sec. III B. In Fig. 7 we compare the polarizability of this cell with the polarizability of the corresponding normal erythrocyte. Again, similar values are found when the external field is aligned with the z axis. However, when the external field is aligned with the y axis the deeper central pallor of the stomatocyte enforces a very different membrane field distribution, especially in the upper half of the membrane. The smaller curvature of the lower half of the membrane produces similar field distributions. It is clear from the results shown in Figs. 6 and 7 that a stomatocyte can not be approximated by an erythrocyte or by a confocal ellipsoid.

For completeness we mention some well-known common features specific to the shelled models (Figs. 3–7) as opposed to the homogeneous particles illustrated in Fig. 2: the imaginary part of the polarizability shows a positive maximum and a negative minimum centered at frequencies f_1 and f_2, respectively; these two frequencies are close to the crossover frequencies f_{c1} and f_{c2} of the real part, and the crossover frequency of the ER spectrum f_{cER} coincides with the frequency f_{DEPmax} of the maximum DEP force [53]. As an illustration, we have marked these frequencies in Fig. 3.

C. Comparison with experimental results

So far, our examples have taken as input the geometric and electric data of the cell, and have given as output the polarizability. The experimental procedure is usually the opposite: relevant cellular parameters like permittivities, conductivities, and area-specific capacitances are obtained from fittings of a theoretical model to experimental ER spectra. We will discuss the experimental results of Becker *et al.* [54], which were obtained with normal erythrocytes immersed in isotonic sucrose of permittivity $\epsilon_1 = 80\epsilon_0$ F/m and conductivity $\sigma_1 = 0.056$ S/m. In Ref. [54] the authors fit a shelled spherical model to their experimental results and obtain precisely the same cytoplasm conductivity and permittivity parameters that we have used in our calculations. They also state that membrane conductance values derived from their analysis were so small that they did not contribute significantly to the measured ER and DEP responses and could not be determined accurately (cf. also Ref. [55]).

Figure 8 shows the experimental points for the imaginary part of the polarizability read off Fig. 2 of Ref. [54], a theoretical curve with the isotonic sucrose medium, and a theoretical curve with our physiological saline (higher conductivity) medium. These two curves provide an additional test of our method, because they reproduce the experimentally well-known effect [53] that f_1 and f_{c1} shift toward lower frequencies when the conductivity of the external medium σ_1 decreases, while f_2 and f_{c2} are much less sensitive to variations in σ_1.

Our calculated polarizability values with the sucrose permittivity follow the same pattern as the experimental results, but although we use a highly resistive membrane, there is a significative difference between the experimental points and the leftmost theoretical curve. We recall, however, that the electrical parameters that we have used for the cytoplasm were calculated by the authors of Ref. [54] by fitting the results of a single-shell spherical model to the experimental data. Therefore this difference is in fact a quantitative measure of the effect of using a realistic erythrocyte shape in the determination of the electric parameters of the cell.

We finally discuss the relative contribution of each term in Eq. (19) to the polarizability. Note that the high conductivity of the cytoplasm (cf. Table I) collapses the electric field
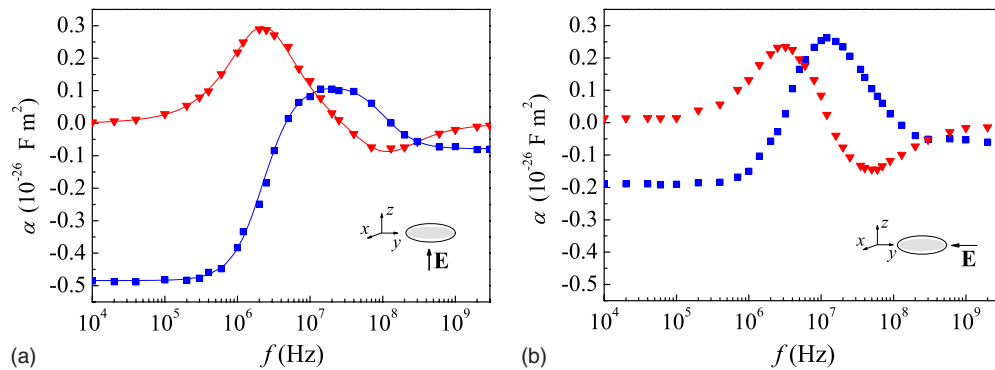

FIG. 5. (Color online) Comparison between the boundary element [solid lines in (a)] and our numerical results for the complex polarizability of a platelet along (a) the minor z axis and (b) the major y axis, as a function of the frequency f of the applied external field. The squares mark the real parts of the polarizability, while the triangles mark the imaginary parts.
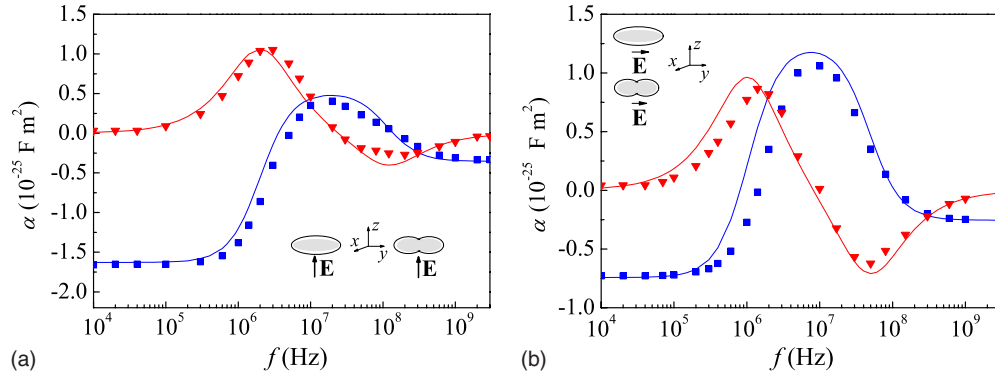
FIG. 6. (Color online) Comparison between our numerical results for the complex polarizability of a realistic model of an erythrocyte and the exact results (solid lines) for an "equivalent" (cf. Sec. III A) confocal ellipsoid along (a) the minor z axis and (b) the major y axis, as a function of the frequency f of the applied external field. The squares mark the real parts of the polarizability, while the triangles mark the imaginary parts.

within this region. Our calculations show that although the volume of the cytoplasm is typically two orders of magnitude larger than the volume of the membrane, the contribution of the membrane to the polarizability is typically one order of magnitude larger than the contribution of the cytoplasm.

V. CONCLUSIONS

Our first result in this paper is a method [Eq. (11)] for the calculation of the complex polarizability of shelled particles of arbitrary shapes in lossy media within the dipole approximation. In the case of a homogeneous particle the induced effective dipole moment can be understood as the product of two medium-dependent factors times the volume of the particle times the average electric field in the particle. In the case of shelled particles, the expression has the form of a weighted average with weights determined by the differences in permittivities between the shells and the external medium. In any event, the calculation of the polarizability is reduced to the calculation of the electric field in the particle, which for all but the simplest shapes can only be obtained with the help of numerical methods. We have used an adaptive mesh

finite-element method which is very effective in handling the irregular domains, material inhomogeneities, and complex boundary conditions usually found in biophysical applications.

After extensive testing with exactly solvable problems, we have applied our method to the calculation of complex polarizabilities of four types of hematic cells: T-lymphocytes, platelets, erythrocytes, and type-II stomatocytes. The first two types can be modeled by a spherical and an ellipsoidal core, respectively, to which we add a uniform thickness membrane. Erythrocytes and stomatocytes have more complex shapes, and we use a set of parametric equations in terms of Jacobi elliptic functions which allow for continuous deformations of the normal erythrocyte into its deformed shape. Again, the use of parametric equations make it a simple matter to add a uniform-thickness membrane. We remark that these shelled models with two interfaces are the simplest structures required to reproduce the maximum and minimum in the imaginary part of the polarizability.

Qualitative aspects of our results can be understood by the continuity at the membrane interfaces (a locus of high-field amplification) of the normal component of the displacement and of the tangential component of the electric field. For
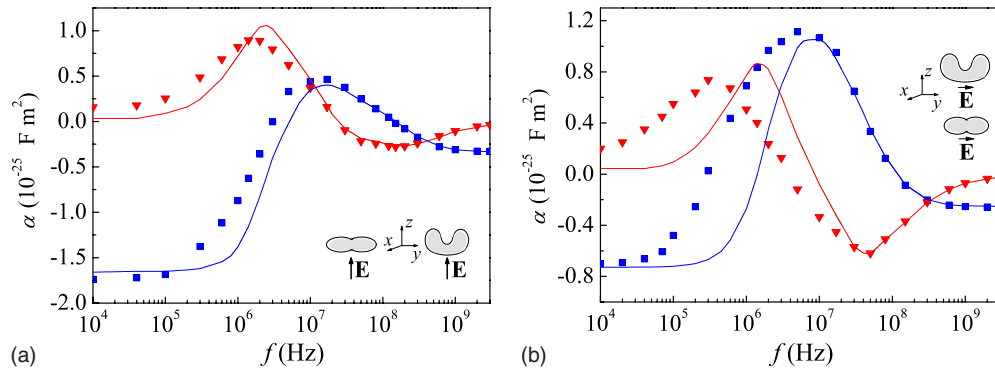

FIG. 7. (Color online) Comparison between our numerical results for the complex polarizabilities of a realistic model of a type-II stomatocyte (markers) and of its precursor normal erythrocyte (interpolated solid lines from the results of Fig. 6) along (a) the minor z axis and (b) the major y axis, as a function of the frequency f of the applied external field. The squares mark the real parts of the polarizability, while the triangles mark the imaginary parts.
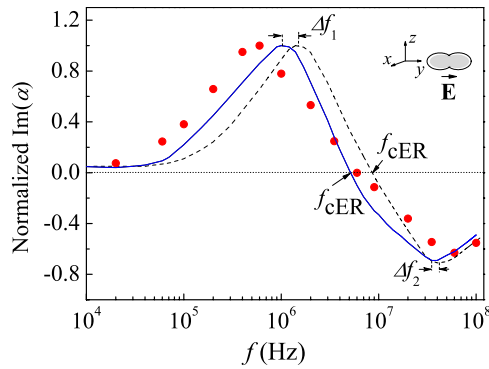
FIG. 8. (Color online) Normalized experimental values (dots) of Becker *et al.* [54] for the imaginary part of the polarizability of a normal erythrocyte in an external isotonic sucrose medium of conductivity $\sigma_1 = 0.056$ S/m and numerical results for the same medium (solid line) and for the physiological saline external medium of $\sigma_1 = 0.12$ S/m (dashed line), as a function of the frequency f of an external field applied along the y axis. This change in conductivity induces a shift Δf_1 in the maximum and a smaller shift Δf_2 in the minimum of the curve.

instance, the polarizabilities of a realistic erythrocyte and of an equivalent (equal diameters and volumes of dielectrics) confocal ellipsoid are very similar along the minor axis, but noticeably different along the major axis. Therefore if the average polarizability is the main concern, a real erythrocyte can be modeled by a confocal ellipsoid. However, if cell

magnitudes such as the membrane field or the transmembrane voltage are to be determined, even the shelled ellipsoid is not a sufficiently good approximation to the real erythrocyte. Similar but more marked differences are found for stomatocytes.

The quantitative effect of a realistic erythrocyte geometry is clearly demonstrated by our comparison of experimental results with numerical calculations performed with electrical parameters obtained from a fitting of the predictions of a shelled sphere model to the very same experimental results. Our calculations also reproduce accurately well-known effects of the conductivity of the external medium on the cell polarizability.

Although our initial motivation to develop this method came from the need to calculate the polarizability of cells which had not been previously addressed because of the limitations of analytical approaches and of the difficulties of accurate numerical computations, our approach is valid for shelled particles of arbitrary shape, is not bound to the finite-element method that we found convenient for our concrete purposes, and can be used successfully, for example, in polarizability calculations for nanoparticles and biomolecules.

[1] C. J. Bottcher, *Theory of Electric Polarization* (Elsevier, Amsterdam, 1952).

[2] J. A. Stratton, *Electromagnetic Theory* (McGraw-Hill, New York, 1941).

[3] M. L. Mansfield, J. F. Douglas, and E. J. Garboczi, Phys. Rev. E **64**, 061401 (2001).

[4] A. G. Ramm, *Wave Scattering by Small Bodies of Arbitrary Shape* (World Scientific, Singapore, 2005).

[5] K. Asami and T. Yonezawa, Biochim. Biophys. Acta **1245**, 317 (1995).

[6] E. Gheorghiu, Ann. N.Y. Acad. Sci. **873**, 262 (1999).

[7] T. B. Jones, IEEE Eng. Med. Biol. Mag. **22**, 33 (2003).

[8] B. K. P. Scaife, J. Mol. Struct. **479**, 285 (1999).

[9] H. Kang and K. Kim, J. Comput. Math. **25**, 157 (2007).

[10] L. Eyges, Ann. Phys. (N.Y.) **90**, 266 (1975).

[11] C. Bohren and D. R. Huffman, *Absorption and Scattering of Light by Small Particles* (Wiley, New York, 1983).

[12] T. Ambjörnsson, S. P. Apell, and G. Mukhopadhyay, Phys. Rev. E **69**, 031914 (2004).

[13] T. Ambjörnsson and G. Mukhopadhyay, J. Phys. A **36**, 10651 (2003).

[14] G. Dassios, M. Hadjinicolau, and G. Kamvyssas, in *Mathematical Methods in Scattering Theory and Biomedical Engineering*, edited by D. I. Fotiadis and C. V. Massalas (World Scientific, Singapore, 2006), p. 128.

[15] D. Vrinceanu and E. Gheorghiu, Bioelectrochem. Bioenerg. **40**, 167 (1996).

[16] J. Gimsa, Bioelectrochemistry **54**, 23 (2001).

[17] N. G. Green and T. B. Jones, J. Phys. D **40**, 78 (2007).

[18] T. B. Jones, *Electromechanics of Particles* (Cambridge University Press, New York, 1995).

[19] M. Sancho, G. Martínez, and C. Martín, J. Electrost. **57**, 143 (2003).

[20] C. Grosse and H. P. Schwan, Biophys. J. **63**, 1632 (1992).

[21] M. Winterhalter and W. Helfrich, J. Phys. Chem. **92**, 6865 (1988).

[22] M. Winterhalter and W. Helfrich, J. Phys. Chem. **96**, 327 (1992).

[23] A. Irimajiri, T. Hanai, and A. Inouye, J. Theor. Biol. **78**, 251 (1979).

[24] K. Asami, Y. Takahashi, and S. Takashima, Biochim. Biophys. Acta **1010**, 49 (1989).

[25] A. D. Michelson, *Platelets* (Elsevier, Amsterdam, 2007).

[26] M. Egger and E. Donath, Biophys. J. **68**, 364 (1995).

[27] B. Neu, R. Georgieva, H. J. Meiselman, and H. Bäumler, Colloids Surf., A **197**, 27 (2002).

[28] D. Sokolowska and J. K. Moscicki, Phys. Rev. E **71**, 031701 (2005).

[29] H. J. Deuling and W. Helfrich, Biophys. J. **16**, 861 (1976).

[30] E. Ponder, *Hemolysis and Related Phenomena* (Grune & Stratton, New York, 1948).

[31] T. L. Steck, in *Cell Shape: Determinants, Regulation and Regulatory Role*, edited by W. D. Stein and F. Bronner (Academic, San Diego, 1989), pp. 205–246.

[32] P. Wong, J. Theor. Biol. **196**, 343 (1999).

[33] T. Auth, S. A. Safran, and N. S. Gov, Phys. Rev. E **76**, 051910 (2007).

[34] G. Lim H. W., M. Wortis, and R. Mukhopadhyay, Proc. Natl. Acad. Sci. U.S.A. **99**, 16766 (2002).

[35] K. D. Tachev, K. D. Danov, and P. A. Kralchevsky, Colloids Surf., B **34**, 123 (2004).

[36] S. Muñoz San Martin, J. L. Sebastián, M. Sancho, and J. M. Miranda, Phys. Med. Biol. **48**, 1649 (2003).

[37] J. L. Sebastián, S. M. San Martín, M. Sancho, J. M. Miranda, and G. Álvarez, Phys. Rev. E **72**, 031913 (2005).

[38] S. Muñoz, J. L. Sebastián, M. Sancho, and G. Álvarez, Bioelectromagnetics (N.Y.) **27**, 521 (2006).

[39] P. Kuchel and E. Fackerell, Bull. Math. Biol. **61**, 209 (1999).

[40] *Handbook of Mathematical Functions*, edited by M. Abramowitz and I. A. Stegun (Dover, New York, 1965).

[41] *ANSOFT HFSS User's Manual* (Ansoft Corporation, Pittsburgh, PA, 2002).

[42] J. Jin, *The Finite Elem ent Method in Electromagnetics* (Wiley, New York, 1993).

[43] J. Douglas, Jr., J. E. Santos, and D. Sheen, Math. Models Meth. Appl. Sci. **10**, 593 (2000).

[44] C. E. Miller and C. S. Henriquez, IEEE Trans. Biomed. Eng. **35**, 712 (1988).

[45] K. Asami, J. Phys. D **39**, 492 (2006).

[46] J. L. Sebastián, S. Muñoz, M. Sancho, G. Álvarez, and J. M. Miranda, Phys. Med. Biol. **52**, 6831 (2007).

[47] D. Giannacopoulos and S. McFee, IEEE Trans. Magn. **30**, 3523 (1994).

[48] G. C. Hsiao, Z. Angew. Math. Mech. **70**, T493 (1990).

[49] C. Liu, D. Sheen, and K. Huang, IEEE Trans. Nanobiosci. **2**, 104 (2003).

[50] R. D. Miller and T. B. Jones, Biophys. J. **64**, 1588 (1993).

[51] J. Gimsa, T. Müller, T. Schnelle, and G. Fuhr, Biophys. J. **71**, 495 (1996).

[52] T. Kotnik and D. Miklavcic, Biophys. J. **79**, 670 (2000).

[53] V. L. Sukhorukov, H. Mussauer, and U. Zimmermann, J. Membr. Biol. **163**, 235 (1998).

[54] F. F. Becker, X.-B. Wang, Y. Huang, R. Pethig, and J. Vyukoukal, Proc. Natl. Acad. Sci. U.S.A. **92**, 860 (1995).

[55] P. R. C. Gascoyne, F. F. Becker, and X.-B. Wang, Bioelectrochem. Bioenerg. **36**, 115 (1995).